Proceedings of the 21st ICSMGE, Vienna, Austria, 14 – 19 June 2026. Pistrol, Adam & Schweiger (eds.)
Published by: ÖGG, Austrian Society for Geomechanics, Salzburg, Austria, ISBN 978-3-9503898-4-5
https://doi.org/10.53243/ICSMGE2026-785

Large deformation modelling of pile installation in clay and comparison with cavity expansion analysis

Lemuel Thompson, Bipul Hawlader
Memorial University of Newfoundland, St. John's, NL, Canada, lythompson@mun.ca

Patrick Staubach
Bauhaus-Universität Weimar, Germany

Kenichi Soga
University of California, Berkeley

ABSTRACT: This paper presents large deformation finite element modelling of the installation of a solid pile in clay. The modified Cam-Clay model is implemented in a Coupled Eulerian Lagrangian finite element program and used to simulate the continuous penetration of the pile. The numerical analyses provide the effective stress components and excess pore water pressure, which cannot be obtained from finite element modelling of undrained penetration in a total stress approach. Analyses are also performed for the commonly used idealized approach of modelling as a cylindrical cavity expansion. Loading–unloading and stress redistribution occur in soil elements near the pile during continuous penetration, while in cavity expansion, the soil elements in the plastic zone near the pile are monotonically loaded along a stress path similar to triaxial compression. The maximum radial effective stress and excess pore water pressure are developed in the soil elements near the pile tip. The steady state effective radial stress and pore pressure, which are less than their respective maximum values, are developed when the pile tip moves deeper past a depth of interest. Stress distribution in the plastic zone at the steady state is different from that obtained from cavity expansion modelling.

KEYWORDS: pile installation; effective stress-based modelling; large deformation; finite element, cavity expansion

1 INTRODUCTION

Large displacement of soil around the pile during installation in clay by jacking or driving changes the stress conditions in the surrounding soil, which could generate significant excess pore pressure and cause remoulding in some cases (Flaate 1972). The penetration-induced excess pore pressure and its subsequent dissipation affect the penetration resistance and the capacity of the pile. Several field campaigns examined the development of excess pore pressures around piles during installation (e.g., Roy et al. 1981, Azzouz and Morrison 1988). For example, Roy et al. (1981) jacked six instrumented steel piles of 203-mm outer diameter into soft sensitive Saint-Alban clay in Québec, Canada. Generated excess pore water pressure (u_e) was measured using a number of piezometers installed at various depths and radial distances from the pile. Negative excess pore pressure was observed when the pile tip was approaching the depth of the piezometer. When the pile tip moved close to the piezometer depth, u_e increased rapidly and reached the maximum when the tip was at the level of the piezometer. With further penetration, the pore pressure reduced and came to a steady value. Azzouz and Morrison (1988) installed 38.4-mm diameter model piles in sensitive Lower Boston Blue clay (BBC) and low sensitive Lower Empire clay. The developed excess pore pressure was measured by placing a piezo-lateral stress (PLS) cell on the pile shaft about 1.8 m behind the pile tip. PLS data shows a significant increase in excess pore pressure and reduction of effective stress. As the shaft friction depends on radial effective stress, proper estimation of excess pore pressure is needed, since it affects the penetration resistance and subsequent load capacity.

Lo and Stermac (1965) developed a simplified analytical solution to estimate the maximum installation induced excess pore pressure. It was assumed that pile installation primarily displaces soil in the radial direction such that within the failure zone, the principal stress is the radial stress (σ_r). The resulting excess pore pressure is composed of the change in the total ambient pressure and increase in shearing stress. The latter component is a function of pore pressure ratio that can be measured in conventional consolidated undrained triaxial tests. This formulation was later observed to underestimate the maximum u_e recorded in field tests (Orrje and Broms 1967; Koizumi and Ito 1967; Clark and Meyerhof 1972; Fellenius and Samson 1976; Roy et al. 1981). Randolph and Wroth (1979) proposed an analytical solution for calculating the pore pressure magnitude and distribution immediately after pile driving, assuming elastic perfectly plastic soil. Reasonable predictions of excess pore pressure can be made, provided suitable values of the secant shear modulus of soil are chosen (Randolph and Wroth 1979).

Large deformation of soil is the major issue in numerical approaches. Several numerical techniques have been developed to model soil behaviour during pile installation. For example, Baligh (1985) proposed the Strain Path Method (SPM), which predicts the 2-dimensional deformation of soil around a 'deep' penetrometer. The solutions provided by the SPM assume the deformation behaviour is independent of the soil properties. Sagaseta et al. (1997) advanced the SPM to account for ground surface effects at shallow depths. Despite these advancements, semi-analytical and empirical methods are still widely used in pile design (Yu, 2000). Among them, the cylindrical cavity expansion theory idealizes the process as the expansion of a cylindrical cavity in an infinite medium. This has been used to model the installation of piles driven into clays (Butterfield and Banerjee 1970, Randolph and Wroth 1979) and the expansion of a cylindrical pressuremeter in both clays and sands (Gibson and Anderson 1961, Ladanyi 1963, Hughes et al. 1977). Note that the cylindrical cavity expansion theory is applicable for modelling the deformation around the pile sufficiently far from the ground surface and pile tip.

Carter et al. (1979) used the cavity expansion theory to estimate excess pore pressure around a driven pile in clay. They assumed the

soil to be elastic perfectly plastic and found that the numerical solution is in close agreement with the analytical solution of Randolph and Wroth (1979). Randolph et al. (1979) used the cavity expansion theory with the elasto-plastic modified Cam-Clay (MCC) and proposed an improved analytical solution to calculate total and effective stress components and generated pore pressure. Azzouz et al. (1990) noticed that the cavity expansion model overpredicts the effective radial stress on the pile shaft by a factor of 2 when compared with the strain path method. This they attribute to the lack of shearing of the soil at the cavity face.

The cavity expansion model does not account for the flow and shearing of soil occurring around the pile during installation. Advanced large deformation modelling techniques like the Remeshing and Interpolation Technique with Small Strain (RITSS), Efficient Arbitrary Lagrangian Eulerian (EALE), and Coupled Eulerian Lagrangian (CEL) techniques, can simulate the soil flow and shearing without mesh distortion issues, and incorporate the effects of the soil's properties on the deformation behaviour. As such, they are suited for studying soil deformation effects during piling, as opposed to the SPM and cavity expansion model. The RITSS, EALE and CEL have been extensively used to simulate a wide range of soil penetration problems (Wang et al. 2008; Staubach et al. 2021; Karmaker et al. 2024). In most of the cases, the analyses were performed for undrained loading conditions. The CEL approach in Abaqus can handle large deformations; however, the built-in models can only simulate the behaviour of single-phase material (e.g., undrained analysis in total stress).

In the present study, the modified Cam clay model (MCC) is implemented and coupled with a hydromechanical model in Abaqus CEL to simulate undrained penetration of a pile in clay. Unlike the total stress analyses, the coupled MCC provides effective stress and pore pressure. Simulations are performed for continuous penetration of pile (full penetration) in a clay layer. Finite Element (FE) modelling is also performed for cavity expansion. The similarities and differences between full penetration and cavity expansion modelling are examined.

2 MODEL SETUP

A solid cylindrical pile of 0.4 m diameter (D) with a half-spherical tip is jacked into a clay layer at a constant velocity to 10 m depth. At any instant, the pile tip is at z_{tip}. The location of a soil element is defined by radial distance r from the pile center and depth z from the ground surface before installation, and the vertical distance h behind the pile tip (Figure 1(a)). To investigate soil response to pile installation, the following two types of finite element analyses are performed.

2.1 FE modelling of cavity expansion

As discussed in the introduction, a number of studies developed analytical solutions to investigate soil response around the pile during installation. It is assumed that the response of soil due to pile installation can be modelled using the cylindrical cavity expansion concept. For modelling, Carter et al. (1979) suggested the expansion of an equivalent cylindrical cavity from an initial radius of $a_0 = R/\sqrt{3}$ to $2a_0$, where R is the radius of the pile.

The cavity expansion is numerically modelled in Abaqus/Explicit FE program. These simulations are also used to validate the user subroutine (VUMAT) developed for the simulation of pile installation. Simulations are performed using a 1.0 m thick soil layer in axisymmetric conditions (Figure 1(c)), as modelled in previous studies (González et al. 2009; Sivasithamparam et al. 2020). The right boundary is sufficiently far from the pile surface (r = $60R$) to avoid any boundary effects on numerical simulation results. The top and bottom boundaries are supported by rollers. Simulations are performed for a soil layer at 5 m depth. Therefore, in-situ vertical effective stress of 40 kPa (= $\gamma' z$) and lateral stress of $40K_0$, are applied to each soil element. A radial stress of σ'_{r0}= $40K_0$ is applied on the right vertical boundary. To simulate cavity expansion, the left boundary is displaced radially from a_0 to $2a_0$ while maintaining quasi-static conditions.

2.2 Modelling of full pile installation

The complete process of pile installation is simulated using the Coupled Eulerian Lagrangian (CEL) approach available in Abaqus software. A quarter of the soil domain is modelled, taking advantage of the axisymmetric nature of the problem (Figure 1(b)). The boundaries are placed sufficiently far from the pile to avoid boundary effects on numerical results. The curved vertical boundary is at 50D from the pile centre, and the bottom boundary is at 125D from the ground surface. A void space of 0.5 m thickness is defined above the ground surface to allow for ground heaving during installation.

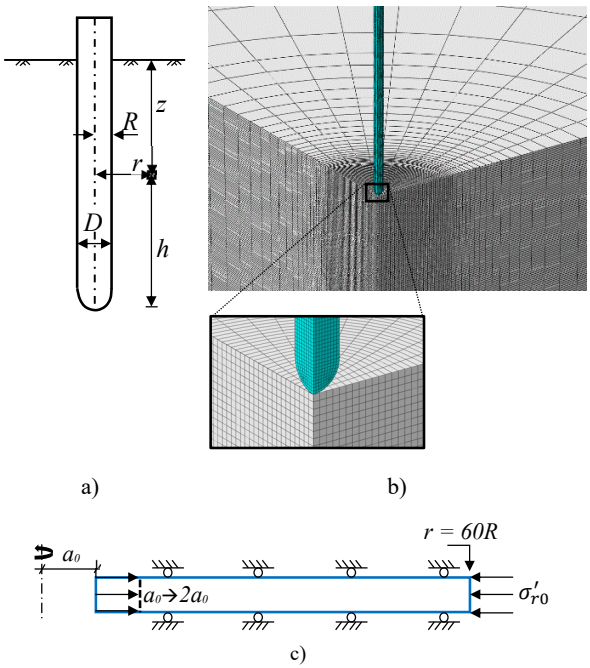

Figure 1. (*a*) Problem definition; (*b*) simulation of full pile installation; (*c*) Cavity expansion modelling.

The void and soil domains are discretized using 3-dimensional hexagonal Eulerian elements with reduced integration (EC3D8R). Finer mesh of ~ 0.1D is used in a zone of 3R radius from pile where significant soil deformation is expected during jacking, as observed

in previous numerical simulations (Qiu and Grabe 2011; Tho et al. 2012; Zheng et al. 2018). The mesh size is gradually increased beyond $3R$ radius, which reduces the number of elements (computational cost) and introduces damping to the model (Staubach et al. 2023). Non-reflecting boundary conditions are defined at the outer boundaries to absorb numerical waves and limit their reflection. The pile is modelled as a rigid Lagrangian body, and is discretized using 8-node 3-dimensional elements with reduced integration (C3D8R). A smooth pile–soil interface condition is used. Zero velocity boundary conditions are applied normal to all the vertical faces, and all velocity components at the bottom are set to zero. Non-reflecting Eulerian boundary conditions are applied at the vertical and bottom boundaries to absorb and limit wave reflections.

FE simulation consists of two steps. First, in the geostatic step, the in-situ stress conditions are established. At this stage the pile tip is slightly above the ground surfaces such that there is no soil–pile interaction. Second, the pile is penetrated at 0.5 m/s to 10 m depth. Jacking rate in the field is generally slower than this (Karmaker et al. 2024). However, as the focus of this study is to model undrained penetration, the simulation at such a slow rate is not required as long as quasi-static conditions are maintained in this type of explicit modelling. This is ensured by maintaining the kinetic energy at less than 2% of the internal energy (Abaqus 2019; Robert et al. 2020).

3 MODELLING OF CLAY

The modified Cam-Clay (MCC) model is used to model clay behaviour, in an effective stress framework. While Abaqus CEL can simulate large deformation, it does not have the MCC as a built-in model. Therefore, the MCC model is implemented in Abaqus by developing a user subroutine VUMAT in Fortran.

3.1 Implementation of MCC in Abaqus CEL

The MCC used is a coupled effective stress based hydromechanical model. Using the MCC model, the change in excess pore pressure ($\dot{\boldsymbol{u}}_e$) is calculated using the method proposed by Britto and Gunn (1987) as $\dot{\boldsymbol{u}}_e = \boldsymbol{D}_w\dot{\boldsymbol{\varepsilon}}$, where $\dot{\boldsymbol{\varepsilon}}$ is the total strain increment and $\boldsymbol{D}_w$ represents the stiffness matrix of the water-air mixture, which is related to the bulk modulus of air-water mixture (K_m) and the soil porosity (n) as:

$$\boldsymbol{D}_w = \frac{1}{n}\begin{bmatrix} K_m & K_m & K_m & 0 & 0 & 0 \\ K_m & K_m & K_m & 0 & 0 & 0 \\ K_m & K_m & K_m & 0 & 0 & 0 \\ 0 & 0 & 0 & 0 & 0 & 0 \\ 0 & 0 & 0 & 0 & 0 & 0 \\ 0 & 0 & 0 & 0 & 0 & 0 \end{bmatrix} \quad [1]$$

The following algorithm is used to implement the MCC model in CEL using the implicit integration approach for elasto-plastic constitutive relations in the FE program (Borja and Lee 1990).

- Enter the subroutine VUMAT with total stress ($\boldsymbol{\sigma}_i$), pore pressure ($\boldsymbol{u}_i$), and total strain increment ($\dot{\boldsymbol{\varepsilon}}_{i+1}$)
- Calculate the effective stresses: $\boldsymbol{\sigma}'_i = \boldsymbol{\sigma}_i - \boldsymbol{u}_i$
- Calculate the new pore pressure: $\boldsymbol{u}_{i+1} = \boldsymbol{u}_i + \boldsymbol{D}_w\dot{\boldsymbol{\varepsilon}}_{i+1}$
- After plastic integration to get the new effective stresses $\boldsymbol{\sigma'}_{i+1}$, calculate and return the new total stresses: $\boldsymbol{\sigma}_{i+1} = \boldsymbol{\sigma'}_{i+1} + \boldsymbol{u}_{i+1}$

where $()_{i+1}$ and $()_i$ refer to quantities at the current and previous time increments, respectively. This is applicable for undrained analysis of fully or nearly saturated soils where consolidation during installation is negligible.

3.2 Geotechnical properties

The soil properties used in this study are same as those used by Randolph et al. (1979) for cavity expansion modelling for pile installation in a clay deposit like Boston Blue clay (BBC). Note that BBC is a sensitive clay (sensitivity of 7 ± 2, Azzouz et al. 1988); however, strain-softening due to sensitivity is not modelled in this study. The MCC model requires the following parameters: *a*) submerged unit weight of the soil (γ'); *b*) earth pressure coefficient at-rest (K_0); *c*) initial void ratio (e_0); *d*) slope of normal compression line in v–lnp' plane (λ); *e*) slope of unloading-reloading line in v–lnp' plane (κ); *f*) slope of the critical state line (M); *g*) maximum mean stress on the initial ellipsoidal yield surface (p'_c); *h*) shear modulus (G); and *i*) drained Poisson's ratio (ν'). Analyses are performed for two soils: A) normally consolidated clay, B) lightly overconsolidated clay of overconsolidation ratio (OCR) of 2. The groundwater is considered at the ground surface. The value of p'_0 (initial mean effective stress) at any depth (z) is calculated as $\gamma' z(1 + 2K_0)OCR/3$. Following the work of Randolph et al. (1979), G is defined as a function of p'_0.

The following parameters are used in numerical simulations: γ' = 8 kN/m^3, ν' = 0.3 e_0 = 1.16, λ = 0.15, κ = 0.03, M = 1.2 and K_m = 50,000 kN/m^2. For Case A, K_0 = 0.55, $G = 36p'_0$, and, for Case B, K_0 = 0.7, $G = 63p'_0$ are used.

4 RESULTS

Several studies conducted large deformation modelling of pile installation in a total stress approach (e.g. Karmaker et al. 2024). In those studies, the change in total stresses (e.g., total radial and vertical stresses) has been examined. In the present effective stress based analysis, the generated pore pressure is also calculated. Therefore, in this section, the change in effective stress components and pore water pressure due to penetration of pile are examined. The results are presented by normalizing the stresses by the undrained shear strength c_u.

4.1 Validation of numerical implementation of MCC

Figure 2 shows the development of total radial stress (σ_r) and pore pressure (u_e) in the soil element next to the cavity with its expansion for both normally and overconsolidated cases (Case A and Case B). As shown, σ_r and u_e increase with radial expansion and the rate of increase becomes small by a/a_0 = 2, which implies negligible change in stresses at this stage. Figure 3 shows the variation of normalized effective radial stress (σ'_r/c_u), tangential stress (σ'_θ/c_u), vertical stress (σ'_z/c_u) and excess pore pressure (u_e/c_u) at the end of radial expansion for Case A. Dashed lines in Figures 2 and 3 show the calculated stresses from the FE solution of Randolph et al. (1979), which match well with FE calculated results (solid lines) of this study. This implies that the MCC model has been properly implemented in the VUMAT subroutine.

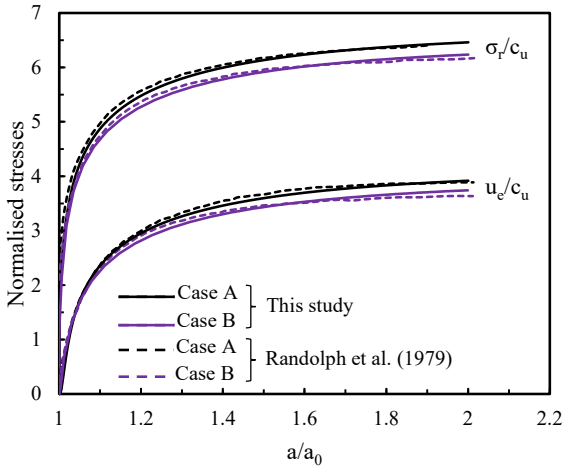

Figure 2. Development of total radial stress and excess pore pressure in a soil element next to the cavity with expansion.

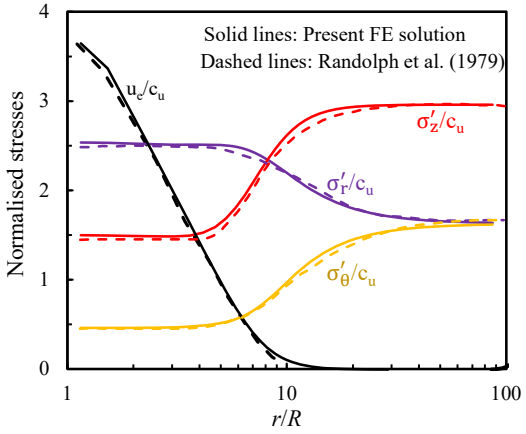

Figure 3. Normalized stress components at the end of cavity expansion.

4.2 *Pile penetration results*

During installation, the soil deformation around the pile tip is similar to the spherical cavity expansion, while it is comparable to cylindrical cavity expansion sufficiently behind the tip (e.g., larger h/R ratio). Figures 4(a) and 4(b) show the variation of stresses with radial distance in soil elements at 5 m depth when the pile tip is at 10 m depth (i.e., h/R = 12.5) for Cases A and B, respectively. As it is sufficiently far from the tip, the FE calculated results can be compared with the cylindrical cavity expansion results previously discussed. Also, these soil elements are sufficiently far from the ground surface; therefore, the shallow failure mechanisms near the ground surface and ground heave are not expected to have a significant effect.

During penetration, plastic shear strain develops in the soil elements near the pile. Based on the equivalent plastic shear strain (ε_q^d) being less than 0.5%, the deformation of the soil elements at 10R far from the pile surface is considered elastic. In other words, soil within a 10R radial distance experiences considerable plastic soil deformation.

Figures 4(a) and 4(b) show a significant difference in calculated effective stresses obtained from full pile penetration and cavity expansion modelling in the plastic zone, especially within 5R for normally consolidated Case A and within 9R for overconsolidated Case B. In this zone, the effective radial and vertical stresses obtained from full penetration modelling are significantly smaller than in cavity expansion modelling, especially in the soil element closer to the pile. An opposite trend is found for effective tangential stress. No significant difference in calculated stresses from full penetration and cavity expansion is found in the zone where low plastic shear strain develops (r/R > 8) and in the elastic zone.

The difference between calculated stresses from full penetration and cavity expansion modelling can be attributed to the difference in loading in these two modelling approaches. Additionally, in the full penetration modelling, a complex flow of soil occurs ahead of and behind the pile as it is installed.

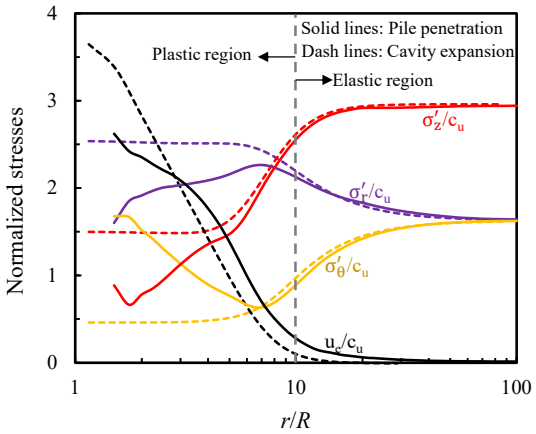

a) Case A

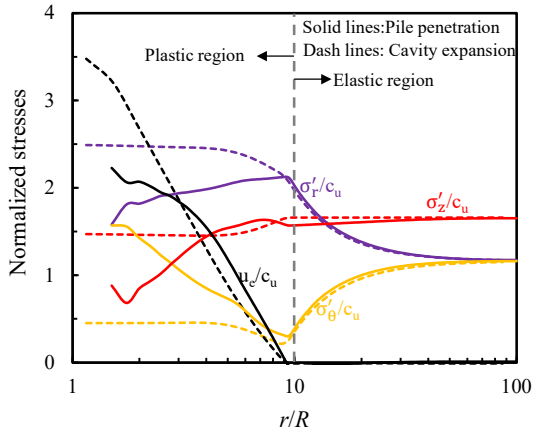

b) Case B

Figure 4. Comparison of stresses in soil elements at 5 m depth obtained from full penetration and cavity expansion modelling.

Figures 5(a) and 5(b) show the normalised radial effective stress and pore pressure during penetration, respectively, in two soil elements at 5 m depth; one close to the pile in the plastic zone at r = 1.5R, and the other one far from the pile in the elastic zone at r =

15R. In these figures, both σ'_r and u_e are normalized by the undrained shear strength of soil at 5 m depth. For the element close to the pile, a negative excess pore pressure is generated as the pile approaches and is maximum when the pile tip is at 3.0 m depth (Figure 5(b)). The effective radial stress slightly increases during this time due to the negative excess pore pressure, before reducing to the lowest when the pile tip is ~1 m above the point of interest (z_{tip} = 4 m). The excess pore water pressure in this soil element increases rapidly when the tip is at 3–5 m, and reaches the maximum when the pile tip is at the depth of the soil element (5 m). The maximum σ'_r is also obtained at this stage. That means both total and effective radial stresses and pore water pressure are the highest when the pile tip is at the depth of interest. σ'_r and u_e in this soil element reduce with further penetration of the pile, and remain almost constant when $z_{tip} > 7$ m. In summary, loading and unloading (in terms of σ'_r) occur in this soil element before coming to a constant value. Roy et al. (1981) measured the variation of pore water pressure in soil elements during the installation of a pile, and reported a similar trend of pore water pressure, shown in Figure 5(b). The dashed line in Figure 5(b) shows a small increase in pore water pressure in the soil element in the elastic zone. In Figure 5(a), the soil element in the elastic zone (dashed line) shows a small variation in effective radial stress with penetration, compared to the element close to the pile.

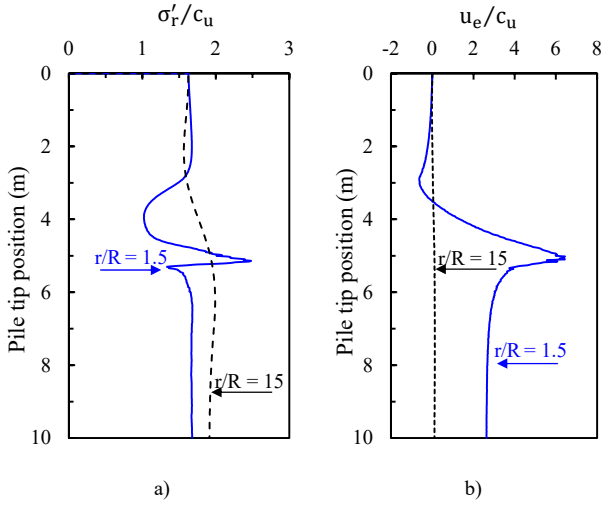

Figure 5. Effective radial stress and pore pressure in two soil elements at 5 m depth with penetration of pile in Case A.

As shown in Figure 2, in cavity expansion modelling, the total radial stress (σ_r) and pore pressure (u_e) increase gradually to the maximum value. This implies that the radial effective stress ($\sigma'_r = \sigma_r - u_r$) is also increased gradually with cavity expansion without any loading/unloading phases as found from full modelling of pile penetration (Figure 5). Also, while the radial effective stress remains constant within 7R in the cavity expansion modelling, it is significantly smaller in the soil elements near the pile for full penetration, before increasing gradually to reach the same value of the cavity expansion model. In other words, the soil flow in full penetration modelling gives different stresses in the soil elements in the plastic zone.

To investigate the difference in stresses obtained from cavity expansion and full penetration modelling in the plastic region, the effective stress path (ESP) of a soil element at 5 m depth and r = 1.5R is plotted in Figure 6. In both analyses, the soil is initially on the yield surface at point A. As the pile approaches the depth of interest, the radial effective stress reduces (Figure 5a), which causes unloading from point A to point B in Figure 6. With penetration, the effective radial stress increases (Figure 5a) and the stress state moves from point B to the initial yield surface and then to point C along a stress path similar to triaxial compression. Point C in Figure 6 represents the stress state when the pile tip is at the depth of interest (5 m).

When the pile tip goes past the depth of the soil element, there is an unloading, as shown in Figure 5(a) for σ'_r, and the stress state moves from C to D (Figure 6). This σ'_r unloading has also been observed by Levadoux and Baligh (1980) in their cone penetration test. The increase in σ'_r due to stress redistribution, as shown in Figure 5(a), increases the deviator stress and moves the stress path from point D to E in Figure 6.

The effective stress path of a soil element at a similar location obtained from cavity expansion modelling is shown by a dashed line in Figure 6. The stress path moves from the initial state A to the critical state line C and then remains constant. The calculated stress path AC is similar to that reported by Randolph et al. (1979) from their FE solution of cavity expansion.

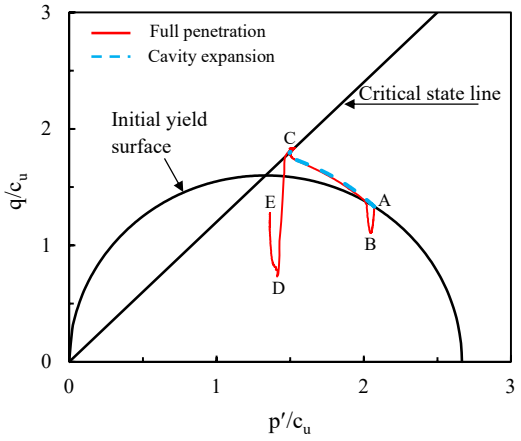

Figure 6. Effective stress path of a soil element in plastic zone obtained from full penetration and cavity expansion modelling.

5 CONCLUSIONS

A numerical method is developed in a coupled effective stress framework to simulate undrained penetration of piles in saturated clay. The analyses are performed by implementing the modified Cam-Clay (MCC) model in the Coupled Eulerian-Lagrangian approach available in Abaqus finite element software. Simulations are also performed for undrained cylindrical cavity expansion with the MCC model. At the end of cavity expansion, the effective radial, tangential and vertical stresses are almost constant in the soil element within a 4R–5R radius; however, these stresses in the full penetration modelling vary with radial distance and are

significantly different from those obtained from cavity expansion near the pile. Such differences result from soil flow around the pile that causes stress redistribution with loading/unloading and plastic deformation, which are captured in the present full penetration modelling. While the general trend of stress variation (e.g., excess pore water pressure) obtained from the present FE analysis is similar to the field observation, further studies are required for direct comparison of numerical simulation results with field data.

6 ACKNOWLEDGEMENTS

The works presented in this paper have been supported by the Natural Sciences and Engineering Research Council of Canada (NSERC).

7 REFERENCES

Abaqus 2019. Dassault Systèmes, Waltham, MA, USA.

Azzouz, A.S., and Morrison, M.J. 1988. Field measurements on model pile in two clay deposits. *Journal of Geotechnical Engineering*, 114(1), 104–121.

Azzouz, A.S, Baligh, M.M., and Whittle, A.J. 1990. Shaft resistance of piles in clay. *Journal of Geotechnical Engineering*, 116(2), 205–221.

Baligh, M.M. 1985. Strain Path Method. *Journal of Geotechnical Engineering*, 1108–1136.

Borja, R.I., and Lee, S.R. 1990. Cam clay Plasticity, Part I: Implicit Integration of Elasto-Plastic Constitutive Relations. *Computer methods in applied mechanics and engineering,* 49–72.

Britto, A.M., and Gunn, M.J. 1987. *Critical state soil mechanics via finite elements,* E. Horwood, Chichester, West Sussex, Uk; Halsted Press, New york, US.

Butterfield, R., and Banerjee, P.K. 1970. The effect of pore water pressures on the ultimate bearing capacity of driven piles. *Proceedings of the Second South East Asian conf. soil Engineering*, Bangkok, 385–394.

Carter, J.P., Randolph, M.F., and Wroth, C.P. 1979. Stress and pore pressure changes in clay during and after the expansion of a cylindrical cavity. *Géotechnique,* 29(4), 361–393.

Clark, J.I., and Meyerhorf, G.G. 1972. The behavior of piles driven in clay. Part I. An investigation of soil stress and pore water pressure as related to soil properties. *Canadian Geotechnical Journal*, 9(4), 351–373.

Fellenius, B.H., and Samson, L. 1976. Testing drivability of concrete piles and disturbance to sensitive clay. *Canadian Geotechnical Journal*, 13, 139–160.

Flaate, K. 1972. Effects of Pile Driving in Clays. *Canadian Geotechnical Journal,* 9(1), 81–88.

Gibson, R.E, and Anderson, W.F 1961. Insitu measurement of soil properties with the pressuremeter. Civil engineering public works Rev., 56, 615–618.

González, N., Arroyo, M., and Gens, A. 2009. Identification of bonded clay parameters in SBPM tests: a numerical study. *Soils and foundations*, 49, 329–400.

Hughes, J.M.O., Wroth, C.P, and Windle, D. 1977. Pressuremeter tests in sands. *Géotechnique*, 27, 455–477.

Karmaker, R., Hawlader, B., Perret, D., and Dey, R. 2024. Numerical Modelling of Pile Jacking in Highly Sensitive Clays. *Canadian Geotechnical Journal,* 61(12), 2597–2614.

Koizumi, Y. and Ito, K. 1967. Field tests with regard to pile driving and bearing capacity of piled foundations. *Soil and Foundation,* 7(3), 30–53.

Ladanyi, B. 1963. Expansion of a cavity in a saturated clay medium. *Journal of the Soil Mechanics and Foundations Division,* 89(4), 127–161.

Levadoux, J.N., and Baligh, M.M. 1980. Pore pressures during cone penetration in clays. *Research report R80-15*, Massachusetts Institute of Technology, Cambridge.

Lo, K.Y., and Stermac, A.G. 1965. Induced pore pressures during pile-driving operations. *Proceedings of the 6th International Conference on Soil Mechanics and Foundation Engineering*, Montréal, Canada.

Orrje, O., and Broms, B.B. 1967. Effects of pile driving on soil properties. *ASCE Journal of Soil Mechanics and Foundations Division*, 93(5), 59–73.

Qiu, G., and Grabe, J. 2011. Explicit modeling of cone and strip footing penetration under drained and undrained conditions using a visco-hypoplastic model. *Geotechnik*, 34(3), 205–217.

Randolph, M.F., and Wroth, C.P. 1979. An analytical solution for the consolidation around a driven pile*. Int. J. Numer. Anal. Meth. Geomech.*, 3, 217–229.

Randolph, M.F., Carter, J.P., and Wroth, C.P. 1979. Driven piles in clay—the effects of installation and subsequent consolidation. *Géotechnique*, 29, 361–393.

Robert, D.J., Britto, A., and Setunge, S. 2020. Efficient approach to simulate soil-pipeline interaction. *Journal of Pipeline Systems Engineering and Practice,* 11(1).

Sagaseta, C., Whittle, A.J., and Santagata, M. 1997. Deformation Analysis of Shallow Penetration in Clay. *Int. J. Numer. Anal. Meth. Geomech.,* 21, 687–719.

Sivasithamparam, N., and Castro, J. 2020. Undrained cylindrical cavity expansion in clays with fabric anisotropy and structure: Theoretical solution. *Computers and Geotechnics*, 120, 103–386.

Staubach, P., Machacek, J., Skowronek, J., and Wichtmann, T. 2021. Vibratory Pile Driving in Water-saturated Sand: Back-analysis of Model Tests using A Hydro-mechanically Coupled CEL Method. *Soils and Foundations,* 61(1), 144–159.

Staubach, P., Tschirschky, L., Machacek, J., and Wichtmann, T. 2023. Monopile Installation in Clay and Subsequent Response to Millions of Lateral Load Cycles. *Computers and Geotechnics,* 155,. 105–221.

Roy, M., Blanchet, R., Tavenas, F., and Rochelle, P.L., 1981. Behaviour of a sensitive clay during pile driving. *Canadian Geotechnical Journal*, 18(1), 67–85.

Tho, K.K., Leung, C.F., Chow, Y.K., and Swaddiwudhipong, S. 2012. Eulerian finite-element technique for analysis of jack-up spudcan penetration. *Int. J. Geomech*., 12(1), 64–73.

Wang, D., Hu, Y., and Randolph, M.F. 2008. Effect of Loading Rate on the Uplift Capacity of Plate Anchors. *Proceedings of the 18th international Offshore and Polar Engineering conference*, Vancouver, BC, Canada, 2, 727–732.

Yu, H. 2000. *Cavity expansion methods in geomechanics,* Springer Science+Business Media, Dordrecht, Netherlands.

Zheng, J., Hossain, M.S., Wang, D. 2018. Estimating spudcan penetration resistance in stiff-soft-stiff clay. *J. Geotech. Geoenvironmental Eng*., 144(3), 04018001–13.